`Supplementary Information

Ultrafast wavefront shaping via space-time refraction

Qingyuan Fan[1], Amr M. Shaltout[2], Jorik van de Groep[3], Mark L. Brongersma[1,2], Aaron M. Lindenberg* [1,4,5]

[1]*Department of Materials Science and Engineering, Stanford University, Stanford, CA 94305*
[2]*Geballe Laboratory for Advanced Materials, Stanford University, Stanford, CA 94305, USA*
[3]*Institute of Physics, University of Amsterdam, 1098 XH, Amsterdam, The Netherlands*
[4]*Stanford Institute for Materials and Energy Sciences, SLAC National Accelerator Laboratory, Menlo Park, CA 94025*
[5]*Stanford PULSE Institute, SLAC National Accelerator Laboratory, Menlo Park, CA 94025, USA*
These authors contributed equally: Qingyuan Fan, Amr M. Shaltout.
** Corresponding author: aaronl@stanford.edu*

S1. Methods

S1.1. Sample preparation

The indium tin oxide (ITO) film is commercially obtained from Honix. The film is 800nm thick, grown by CVD on a glass substrate. The ITO film is cleaned by sonicating in acetone twice and in isopropyl alcohol at $40\,^{\circ}C$, then blow dry for the thermal process. Annealing the ITO film in a forming gas atmosphere at $300\,^{\circ}C$ for 18 min, the ENZ wavelength is tuned to ~1550nm.

S1.2. Experimental setup

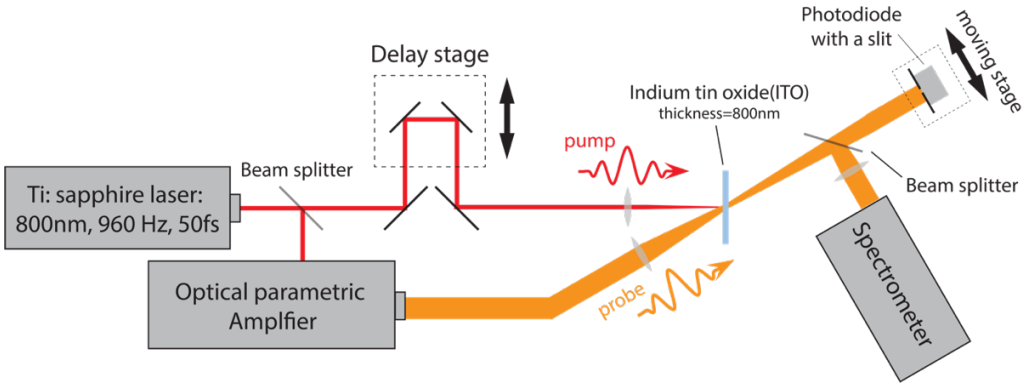

Figure S1 Experimental setup

As shown in Figure S1, a pump-probe setup is used to investigate the transient frequency conversion and beam deflection. Laser pulses with duration of 55 fs (full width at half maximum, FWHM) at 800 nm are generated from a Ti:sapphire mode-locked laser. A beam splitter is used to separate a fraction of the energy as pump pulses, while guides another fraction to pump an oscillating parametric amplifier (OPA) to generate wavelength-tunable near IR probe beams with a bandwidth of ~ 40nm FWHM. The pulse repetition rate is 960 Hz. The sample is mounted on a rotation stage to control the incident angles of both pump and probe beams. Re-alignment of the pump beam is needed if pump-probe angle needs to be adjusted.

Transmitted and reflected probe beam are guided into a monochromator with a photodiode receiving the output photons. By scanning the monochromator in wavelength, changing the incident angle of probe by rotating the sample and switching the polarization direction of the probe by rotating a half-wave plate in the probe path, the transmissivity and reflectivity as a function of wavelength, incident angle and polarization direction are collected.

To characterize the beam steering in space, the transmitted probe beam is collected by a photodiode, masked with a vertical slit with width of 100 μm (Figure S2). The photodiode is movable in the transverse direction of the probe beam on a stage. The photodiode is at 43.15 cm downstream from the sample, which provides a spatial resolution on the order of 100 μm and an angular resolution on the order of 0.003 rad. By scanning the photodiode, the distribution of the transmitted beam spot is obtained, which indicate the central position (refraction angle) and the width in space (divergent angle) of the transmitted probe beam. The transient refraction angle and divergent angle is obtained by collecting data at different pump-probe delays (Figure S3g).

S2. Characterization of dielectric properties

S2.1. Static refractive index

As a transparent conducting oxide (TCOs) material, ITO has permittivity matching well with the Drude model [1]:

$$\epsilon(\omega) = \epsilon_\infty - \frac{\omega_p^2}{\omega^2 + i\omega\gamma} \qquad (S1)$$

where the background permittivity ϵ_∞, plasma frequency ω_p and the damping coefficients γ are three parameters to determine the dielectric properties of the materials, and to determine the permittivity together with the wavelength ω. Wavelength dependent transmittance and reflectance at different incident angle (10 to 45 degrees) and polarization directions (TE and TM) are experimentally measured (Figure S2).

A transfer matrix method (TMM) combined with least-square fitting is used to obtain the Drude parameters. We calculated the transmittance $T_{cal}(\omega, \theta, \epsilon_\infty, \omega_p, \gamma, r)$ and reflectance $R_{cal}(\omega, \theta, \epsilon_\infty, \omega_p, \gamma, r)$ by applying TMM to a multilayer structure, consisting of air, an 800 nm thick ITO film with given Drude parameters ($\epsilon_\infty, \omega_p, \gamma$), a 0.55 mm thick quartz with index of 1.42 and air, at different frequency ω, incident angle θ and polarization direction (r=TE/TM). Results are obtained by minimizing square of error χ^2 between calculated and measured results:

$$\min_{\epsilon_\infty, \omega_p, \gamma} \chi^2 = \min_{\epsilon_\infty, \omega_p, \gamma} \sum_{\omega, \theta, r} [(T_{cal} - T_{measure})^2 + (R_{cal} - R_{measure})^2] \qquad (S2)$$

Fitted results give $\epsilon_\infty = 4.9$, $\omega_p = 2.76 \times 10^{15}$ rad/s and $\gamma = 2.5 \times 10^{14}$ rad/s.
Permittivity is as given in Figure S2c in the main text.

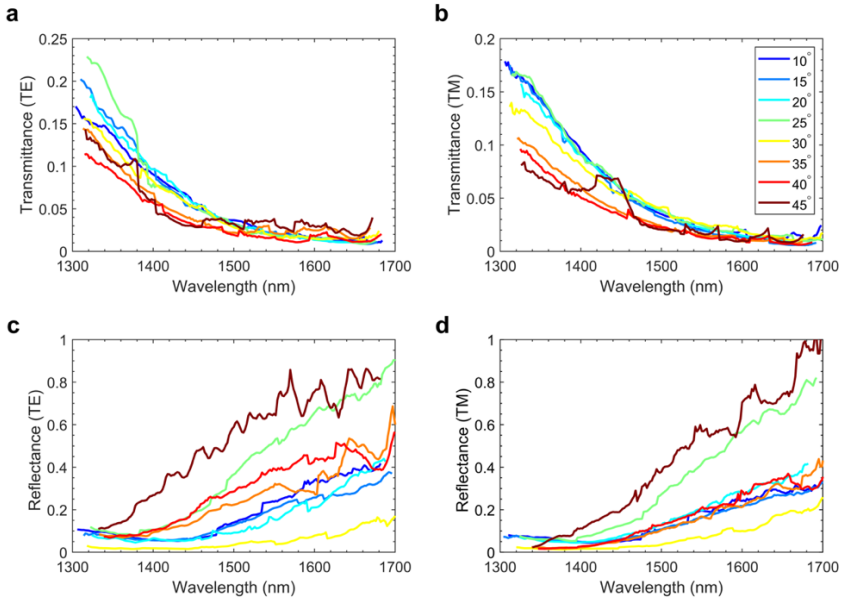

Figure S2 Wavelength dependent transmittance and reflectance are measured at different incident angles (10°,15°, 20°, 25°, 30°, 35°, 40°, 45°) and polarization directions (Transverse Electric, TE, and Transverse Magnetic, TM).

S2.2. Dynamic refractive index modulation

To obtain the dynamic refractive index change induced by the pump pulses, the transient transmittance $T(t,\omega)$ and reflectance $R(t,\omega)$ are experimentally collected at 6 different wavelengths from 1460 nm to 1660 nm (Figure S3a-f), by scanning the pump-probe delay. The same method as in S2.1 is used to fit the time dependent Drude parameters (plasma frequency ω_p, Figure S3g and damping coefficients γ, Figure S3h). The calculated Drude parameters gives the refractive index as function of wavelength and pump-probe delay, $n(t,\omega)$. Fitted refractive index at the wavelength 1540nm is shown in Figure S2c (top). The changing rate of refractive index, Figure S2c (bottom), is obtained from the difference of the transient index change.

S3. Beam steering induced by spatial gradient of refractive index

The ultrafast wavefront steering is induced by the spatial-temporal refractive index gradients generated by the pump pulse. In this section, we will explain the spatial-temporal modulation of refractive index, and the principles of wavefront steering and frequency shift. Beam deflections by an inhomogeneous refractive index that contributes to different phase change for beams propagating through different positions of a film are well known [2-4]. As indicated by Huygens' principle, the wavefront is the plane where the phase of the waves are equal, which determines the propagation direction of the beam. As a general form of Snell's law, the momentum of the probe is modified by the spatiotemporal gradient that the pump induces to the ITO [5]:

$$k_t \sin\theta_t = k_i \sin\theta_i + \frac{\partial\varphi}{\partial x} \qquad (S3)$$

where $k_i = \omega_i/c$ and $k_t = \omega_t/c$ are the wavenumbers of the incident and transmitted probe beam, and $\frac{\partial\varphi}{\partial x}$ is the spatial gradient of the phase-shift imparted onto the probe beam along the

ITO surface. The term $\frac{\partial \varphi}{\partial x}$ is determined by the space gradient of the refractive index.

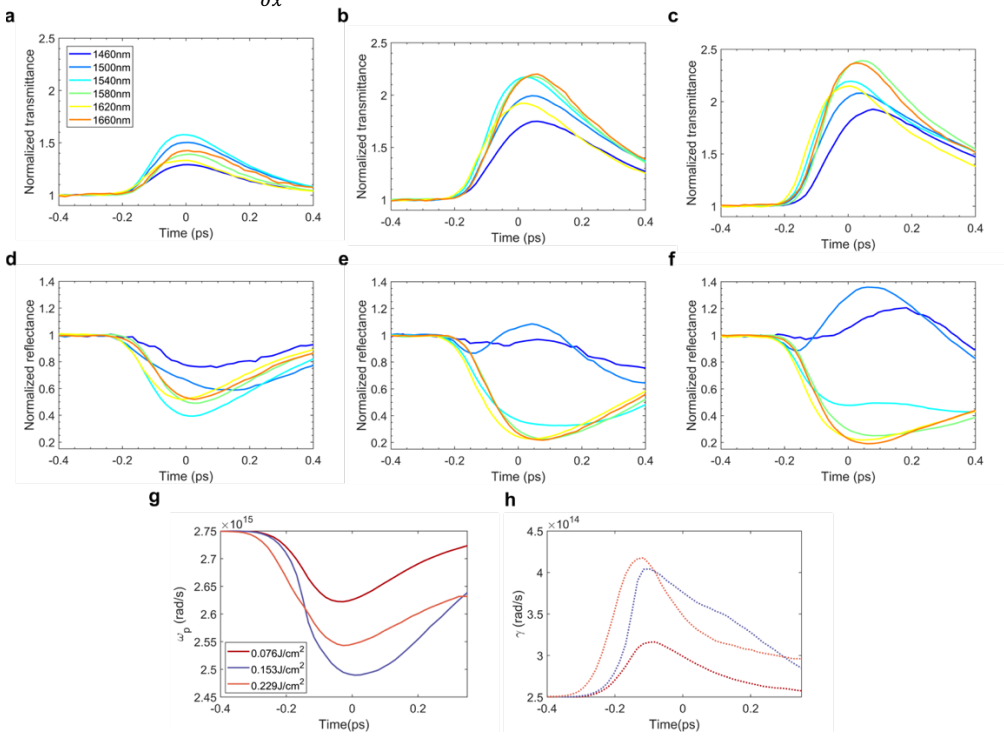

Figure S3 Transient transmittance (a-c) and reflectance (d-f) with the pump fluence of 0.08J/cm^2 , 0.15J/cm^2 and 0.23J/cm^2 , and calculated plasma frequency ω_p (g) and damping coefficients γ (h) as a function of pump-probe delay.

Now we explain the generation of the space gradient of the refractive index. The large spatial gradient of the refractive index is established under the ultrafast index response to the pump pulses. Photons in the pump pulses are absorbed and inject hot carriers, inducing the dynamic change of refractive index, which can be expressed by $n(t)$, indicated by Figure S2b,c in the main text. The ITO film contributes only a small absorption of the 800 nm pump pulses (less than 10% when incident angle is smaller than 35degrees), which implies negligible fluence difference experienced by the medium at different depths. At any point in time, two points separated by an interval of $\Delta z'$ have a time delay difference of $\Delta t = \Delta z'/v_{g(pump)}$, where $v_{g(pump)}$ is group velocity of the pump and $\widehat{z'}$ is direction of pump propagation direction. The amplitude of the index gradient is given by:

$$\nabla n = \frac{\partial n}{\partial z'} = \frac{\partial n}{\partial t} \cdot \frac{\partial t}{\partial z'} = \frac{1}{v_{g(pump)}} \frac{\partial n}{\partial t} \tag{S4}$$

which is equation (3) of the main text. The direction of the spatial gradient is aligned with the propagation direction of the pump pulse. The refraction angle of the pump beam in the ITO film, θ'_{pump}, is given by $\sin(\theta_{pump}) = n_{pump}\sin(\theta'_{pump})$. Thus, the gradient of the index along the ITO surface is:

$$\frac{\partial n}{\partial x} = |\nabla n| \sin(\theta'_{pump}) = \frac{1}{v_{g(pump)}} \frac{\partial n}{\partial t} \frac{\sin(\theta_{pump})}{n_{pump}} \tag{S5}$$

The phase gradient term $\partial\phi/\partial x$ in equation (S3) can be written:

$$\frac{\partial \phi}{\partial x} = \frac{2\pi}{\lambda}\frac{\partial n}{\partial x}\delta z = \frac{2\pi}{\lambda}\frac{1}{v_{g(pump)}}\frac{\partial n}{\partial t}\frac{\sin(\theta_{pump})}{n_{pump}}\delta z \quad (S6)$$

With these simplifications, equation (S3) can be written as:

$$k_t \sin\theta_t = k_i \sin\theta_i + \frac{2\pi}{\lambda}\frac{1}{v_{g(pump)}}\frac{\partial n}{\partial t}\frac{\sin(\theta_{pump})}{n_{pump}}\delta z \quad (S7)$$

where δz is the thickness of the thin film. This equation can be applied at any arbitrary plane within the ITO and integrated over the film thickness, enabling calculation of the beam steering magnitude.

In order to calculate the wavefront steering magnitude more intuitively, it's equivalent to set the refraction interface in equation (S7) perpendicular to the propagation direction of the probe. By defining the angle between the index gradient and probe propagation direction as θ_{pp}, a gradient of index along the interface is:

$$\frac{\partial n}{\partial x'} = \frac{|\nabla n|}{n}\sin(\theta_{pp}) \quad (S8)$$

As shown in Figure S4, a probe beam transmits through a layer of a material with the index gradient of $\frac{dn}{dx}$, and thickness of L. With a space interval of Δx, the refractive index has a difference of $\Delta n = \Delta x\ dn/dx$. The light travel path through the film has a difference of $\Delta D = L\Delta x\ dn/dx$. As Fermat's Principle suggests, the wavefront, the plane with equal phase, is shaped by the light travel difference. The deflection angle is given by:

$$\delta\theta = \frac{\Delta D}{\mathrm{n}_0 \Delta x} = \frac{L}{n_0}\frac{dn}{dx} \quad (S9)$$

where n_0 is the refractive index of the output medium. Combining equation (S4, S8 and S9), the beam will be deflected by an angle of:

$$\delta\theta_{probe} \approx \sin\delta\theta_{probe} = \frac{|\nabla n|}{n_o}\sin(\theta_{pp}) \times \delta l = \frac{1}{v_{g(pump)}}\frac{1}{n_o}\frac{\partial n}{\partial t}\sin(\theta_{pp}) \times \delta l \quad (S10)$$

on a travel distance of δl, which is equation (4) in the main text. In actuality, the result is more complex because the value of refractive index n_0 and the changing rate of refractive index $\partial n/\partial t$ can vary within the film. The angle between pump and probe θ_{pp} can also change as the probe beam is continuously steered. Equation (S10) is only applicable when the propagation distance δl is small enough to ignore the change of n_0, $\partial n/\partial t$ and θ_{pp}. So, the angle deflection on the sample will be the integral over the beam path:

$$\Delta\theta_{probe} = \int_{\delta l} \delta\theta_{probe}(t) \quad (S11)$$

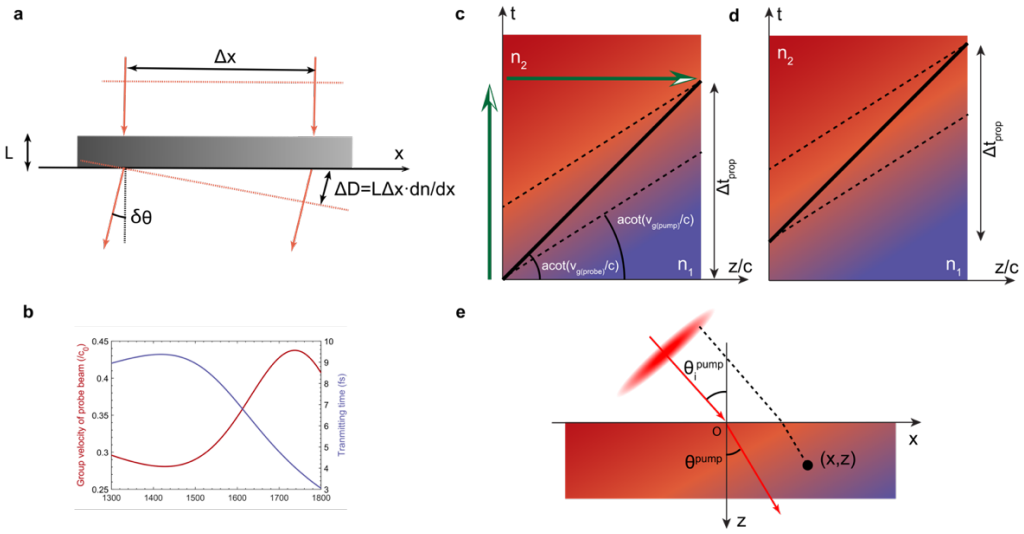

Figure S4 a Diagram of beam steering on a film with spatial index gradient dn/dx. Dashed lines indicate wavefronts of the beam. Within a distance Δx, light travel difference generated is ΔD, which corresponds to a distance of $\Delta D/n$ where n is the index in the o-utput medium. b Group velocity and the time that probe photons travel in the film when normally incident.c,d Refractive index as a function of position and time. The black solid line shows the propagation of the probe beam, while the black dashed lines indicate the line with equal refractive index. The slopes of the solid and the dashed lines are ratio between group velocity of the probe and pump beam, respectively, over the light speed. c and d demonstrate two probe photons which arrive at the ENZ film with a time interval. e Diagram of the light pulse propagation. The time that the pulse arrives at a position is determined by the geometric parameters, including the position coordinate and the incident angle.

The temporal changing of the refractive index also contributes to the wavefront steering by shifting frequency of the photons. It has been studied both theoretically and experimentally that the frequency of photons can be shifted when they propagate in a material with temporally varying refractive index [6-8]. The frequency shift is calculated by:

$$\delta\omega(t) = -\frac{\omega}{n_g}\delta n(t) \tag{12}$$

where n_g is the group index of the material.

In Fig. 1c in the article, the modulation of both momentum and frequency is described. The wavefront steering effect from temporal index change is achieved by accumulating the frequency shift in the film, and shows up when probe beam exits the film.

In process 3 in Fig 1. C, when a photon leaves the ITO film and exits into the air, the frequency has been modulated and becomes different from the frequency when it reaches the ITO film. The refraction angle at the ITO-air interface is determined by both the tangential momentum value before the interface, and the momentum magnitude after the interface. With the same determined tangential momentum, as a comparison, the refraction angle in a static system should be pointing to the iso-frequency curve indicated by the blue solid line, with the same radius with the incident beam. Taking frequency shift into consideration, with frequency shift, the momentum points to the new iso-frequency contour (blue dashed line). The difference of the refraction angle from the solid iso-frequency contour to the dashed contour in process 3

indicates the contribution of the wavefront steering from frequency shift generated by temporal index modulation.

In the end of the discussion on principles, we would like to make a conclusion on the light modulation with spatial-temporal refractive index gradients. In this space-time 4D system, the effects can be separated into three aspects: 1) frequency shift induced by the temporal index change, ($\Delta\omega \neq 0, \Delta|\mathrm{k}| = 0, \Delta\theta_k = 0$); 2) momentum magnitude change induced by the spatial index gradient along the probe beam propagating direction ($\Delta\omega = 0, \Delta|\mathrm{k}| \neq 0, \Delta\theta_k = 0$); 3) wavefront (momentum direction) steering induced by the spatial index gradient perpendicular to the probe beam propagating direction, ($\Delta\omega = 0, \Delta|\mathrm{k}| = 0, \Delta\theta_k \neq 0$).

The effect 3), wavefront steering has been demonstrated in Fig. 1c and Figure S4a. The effects 1) and 2) are discussed in Figure S4c,d, the time and space variant refractive index. Here the axis z' is the direction of the probe beam propagation. For simplicity, the pump and probe beam are assumed to propagate in the same direction. As the refractive index modulation is induced by the pump pulses, the iso-refractive-index position should move with the same velocity of the pump pulses. Figure S4c,d, the slope of the dashed line indicates the group velocity of the pump. The back solid line indicates the propagation of the probe beam, with a slower group velocity of the pump beam. This is because the group index in ENZ range of ITO is larger than that at 800 nm. The refractive index change that the probe pulse experience is the index difference between the two dashed lines. It includes two processes indicated by the two green arrows: temporal index increasing (vertical) and index change when it propagates in the material with a spatial gradient in the index (horizontal). The temporal change corresponds with effect 1) mentioned above which contributes to frequency shift, while the horizontal index change contributes momentum magnitude change. Here, Figure S4c and Figure S4d refers to two positions of a probe beam, with different pump-probe delay, for example, position A and B in Fig. 1a as the pump pulses arrive at these positions with a time interval. For the probe rays at the difference positions, although they experience similar index temporal variation (color change in Figure S4c,d), the overall index that they experience is different (more reddish in Figure S4c, closer to n_1, while more blueish in Figure S4d, closer to n_2), which contribute to a phase difference in space, inducing wavefront shaping

S4. Simulation of wavefront steering and frequency shift for real pulses

The simulation to calculate the wavefront steering and frequency conversion includes the calculation for each photon and averages over all photons in a pulse. When studying a single photon, the deflection angle through a small distance is determined by equation (4, S10). To calculate the result for an 800nm film, we need to know the refractive index distribution and its gradients at any given time and position. As indicated in Figure S4e, $t = 0$ is determined to be the time that the center of the pump probe arrives at the sample surface. With a given incident angle θ_i^{pump} and the refractive index n_{800nm} =1.42 of the pump beam, the time that the wavefront arrives at a position in the ITO film with the thickness z and tangential position x, $t\left(\theta_i^{pump}, z, x\right)$, can be obtained by geometric calculation. With the calculated arrival time $t\left(\theta_i^{pump}, z, x\right)$ and the characterized dynamic index change $n(t)$ in Fig. 2b, the distribution in time and space is expressed by $n\left(t\left(\theta_i^{pump}, z, x\right) + t_{delay}, \lambda_{probe}\right)$, which is numerically known in the simulation.

The original parameters of a probe photon are its wavelength λ_{probe}, incident angle θ_i^{probe}, tangential position x, and the pump-probe delay t_{delay}. With the similar geometric calculation as above, the time that it arrives at a given position is obtained by $t\left(\theta_i^{probe}, z, x\right)$. Here the local pump-probe delay is given by:

$$\tau = t\left(\theta_i^{probe}, z, x\right) - t\left(\theta_i^{pump}, z, x\right) + t_{delay} \quad (S13)$$

which provides the information to determine the refractive index, $n(\tau, \lambda_{probe})$.

We cut the ITO film into m layers, with thickness 800/m nm for each layer. Firstly, we calculate the refraction angle, θ_{probe},at the air-ITO interface, which is the refraction angle in the first layer. We calculated the propagation distance by $\delta l = (800/m)\text{nm}/\cos(\theta_{probe})$. This gives all parameters needed in equation (S4) to calculate the wavefront shaping and to update the refraction angle in the next layer. We also calculated the propagation direction in this layer by $\delta t = \delta l / n_g(\tau)$, where $n_g(\tau)$ is the group velocity at the given time delay and probe wavelength, that provides temporal index change by $\delta n = \partial n/\partial t \cdot \delta t$. With the index change and equation (5), we obtain the frequency conversion value and update the wavelength as well as the corresponding index in the next layer. The above process is integrated over the ITO film. Finally, Snell's law is applied on the ITO-air interface to give the result for the refraction angle.

We note that the dynamic index change happens on 100 fs time-scales, which is tens of micrometers in space. Therefore it's reasonable to assume that the refractive index and its changing rate don't change much over a distance of nanometers, so it's accurate to integrate on the δl of nanometers. We set the value of m to be 80 in the simulation.

The simulated results of the frequency conversion and wavefront steering are indicated in Figure S5a,b, when the pump-probe delay is adjusted to maximize the space-time refraction. When the probe beam is at normal incidence, the frequency conversion is almost independent of the incident angle of the pump beam, while the beam steering magnitude is in positive correlation with the pump angle. It can be interpreted that when the incident angle of the pump increases, the angle between the probe beam and space gradient of index increases. It gives an increasing projection of the space gradient of index on the transverse direction of the probe, and enlarges the wavefront steering. In the condition with normally incident pump beam, frequency conversion increases with the incident angle of the probe beam. This is because the propagating distance and the light-matter interaction time are increased when the probe beam is obliquely incident on a film. It also makes the beam steering effect increase more sharply, compared with the pump-angle-dependent curve.

However, in actual measurements with femtosecond pulses, it's necessary to consider the spatial and temporal distribution of a pulse, because the beam spot is not an ideal point. When obliquely incident, photons at different parts of the probe beam arrive at the sample surface at different time delays, experiencing different amplitudes of the spatiotemporal gradient of index. To have a better sense of this effect, a few values are given below: though the group velocity at ENZ wavelength can be as slow as around 0.28*c,* the time for a photon to transmit through an 800 nm thick ITO film is on the order of 10 fs (Figure S4b). In the temporal behavior of the refractive index change, the FWHM of the dn/dt peak is around 70 fs as shown in Fig. 2b,

which means that each photon only experiences a small fraction of the total index change. Specifically for our setup, the spatial width of the probe beam is $w = 35\mu m$ (FWHM), while the pump beam is large enough ($> 250\mu m$) compared with probe. As demonstrated in Figure S5g,h, when obliquely incident, there is a time interval Δt that two ends of the probe beam have in temporal index change. The arrival time distribution of the probe pulse can be calculated by:

$$\Delta t = \frac{w}{c}\tan(\theta_{probe}) \tag{S14}$$

$$\Delta t = \frac{w}{c}\sin(\theta_{pump}) \tag{S15}$$

where θ_{probe} and θ_{pump} are the incident angles of the probe and pump beam. At a probe angle of 40°, two points on the probe spot with an interval of $w = 35$ μm arrive at the sample with a time interval of 98 fs, which is large compared with the FWHM of the dn/dt peak of 70 fs. This time interval means that even with optimal pump-probe delay, only photons in the middle part of the beam spot can take advantage of the fastest index change and largest index gradient, while the two tails of the beam spot significantly lower the averaged $\delta\omega$ and $\delta\theta_{probe}$.

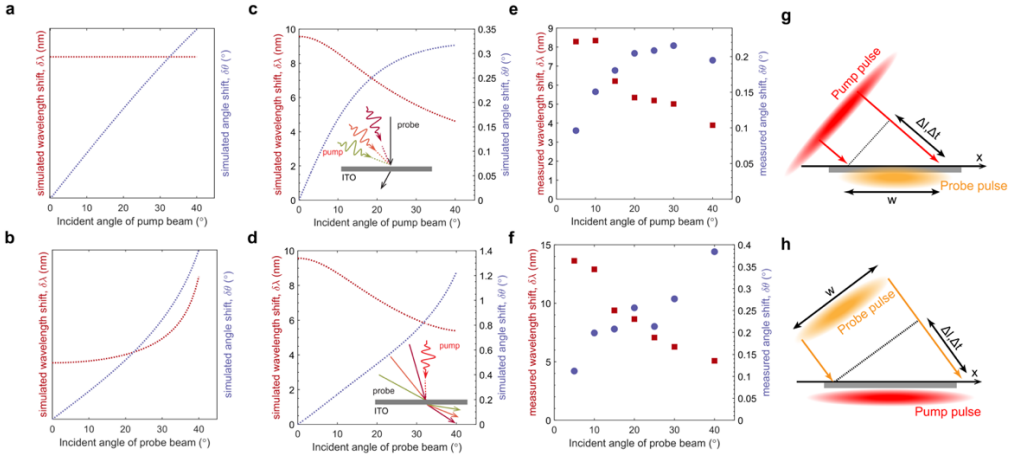

Figure S5 In two conditions with normally incident probe beam (top) and normally incident pump beam (bottom), the incident pump angle (top) and probe angle (bottom) dependent frequency shift (blue) and beam deflection (red) amplitude is simulated and measured: a,b Calculated frequency shift and angle shift from Eqn(3) and (5) which doesn't consider spatial and temporal distribution of photons in a pulse. c,d Simulated averaged frequency shift and angle shift of a pulse, considering consider spatial and temporal distribution. e,f Measured results.g,h Diagram of pulse propagation before the sample. w is the FWHM of probe beam spot size. Δl and Δt are the beam path difference and time interval respectively, that two sides of the probe beam overlaps with pump beam, which indicates different time delay in temporal index change.

We assume probe pulses are Gaussian in both time and space with an energy distribution $I(t', x', y') = I_0 \exp\left(-\left(\frac{x'^2}{w^2} + \frac{y'^2}{w^2} + \frac{t'^2}{\tau^2}\right)\right)$, where w and τ are 35 μm and 33 fs respectively. In other words, the time distribution of the energy is the spatial distribution on the wave packet propagation direction. Photons have the distribution probability as indicated by $I(t', x', y')$.The time delay of the photons with respect to the pump can be calculated with the method as indicated in Figure S4c. For a given (t', x') set, beam steering is given by:

$$\delta\theta(t', x') = \int dl \cdot \frac{|\nabla n|}{n} \sin(\theta_{pp}) \tag{S16}$$

while the averaged beam steering amplitude is

$$\langle \Delta\theta \rangle = \frac{\int_{t',x'} \delta\theta(t', x') \cdot I(t', x')}{\int_{t',x'} \mathrm{I}(t', x')} \tag{S17}$$

The refraction at the interfaces is also considered in the final results. The frequency shift is calculated in a similar way with equation (1) and

$$\langle \Delta\omega \rangle = \frac{\int_{t',x'} \delta\omega(t', x') \cdot I(t', x')}{\int_{t',x'} \mathrm{I}(t', x')} \tag{S18}$$

Taking this beam spot size and the incident angle related effect into simulation, results for realistic pulses are plotted in Figure S5c,e, which fits the measured results well. For the probe angle dependent effect, the frequency shift decreases slower than the varying pump angles because the propagation time in ITO is increasing with the incident angle. The angle shift is monotonically increased, instead of saturating and decreasing for varying pumping angles as suggested by equations (4) and (5). The simulated results can be overestimated because the index change is fitted with data measured at 15 degrees, which may also have the effect of blurring, giving slower temporal index response than reality.

S5. Ultrafast lensing effect

S5.1. Modeling of ultrafast lensing effect

Ultrafast non-reciprocal beam steering by pumping ENZ films opens up novel opportunities to manipulate light by tuning the incident angle and time delay. As mentioned in equation (3, S4), the beam deflection amplitude is proportional to the sine of the angle between pump and probe in the ENZ materials. This indicates that the local wavefront can be engineered or modulated by the incident angle of a control beam. A direct way is to generate divergent or focused pump beam with a common lens, which has a local incident angle that is zero at the beam spot center and increases in the radius direction. A shown in Fig 4.a in the main text, by locating a sample at a distance of z_0 away from the focal point of the pump, the incident angle can be expressed as:

$$\theta_{pump}(x) = arc\tan\left(\frac{x}{z_0}\right) \tag{S19}$$

where the x axis is the radius direction in the plane of sample, with the center of the pump beam at $x = 0$. In this case with a normally incident pump beam, the incident angle is zero in the center of the beam spot, and increases in the radius direction. The deflection angle can be calculated via:

$$\theta(x) = \frac{\nabla n}{n} \cdot L \cdot \sin\left(\theta_{pump}(x)\right) = \frac{1}{v_{g(pump)}} \frac{\partial n(t+\tau)}{\partial t} \cdot L \cdot \sin\left(\theta_{pump}(x)\right) \tag{S20}$$

which is proportional to $\sin\left(\theta_{pump}(x)\right)$ at a given pump-probe delay. Within a small angle approximation, $\tan\left(\theta_{pump}(x)\right) \approx \sin\left(\theta_{pump}(x)\right) \approx \theta_{pump}(x)$ when $\theta_{pump}(x) \ll 1$. With paraxial approximation, the radius distribution of the pump beam spot is small, with $x \ll z_0$. The distance from the focal point to different areas of the sample is $l(x) = \sqrt{x^2 + z_0^2}$. When the distance z_0 is much larger than x, the difference in the distances to the focal point $l(x)$ is negligible. Then the deflected angle of probe can be expressed as:

$$\theta(x) \approx \frac{1}{v_{g(pump)}} \frac{dn}{n\, dt} \cdot L \cdot \frac{x}{z_0} \tag{S21}$$

The photons in the beam at different distances x to the spot center of pump will be focused at the optical axis $\hat{z}$ at the distance of $z(x)$ away from the ITO film given by:

$$z(x) = \frac{x}{\tan\big(\theta(x)\big)} \approx \frac{n\, z_0}{\nabla n \cdot L} \equiv f \tag{S22}$$

Here the focused distance $z(x)$ is independent of the position on the ENZ film. It means that with the small angle approximation and paraxial approximation, all the light with be focused on one point.

We further simulated the ultrafast focusing effect. When the pumping fluence is $0.23\mathrm{J/cm^2}$, the value of $\frac{1}{v_{g(pump)}} \frac{\partial n(t+\tau)}{\partial t}$ in equation (S5) is determined from dynamic refractive index fitted from the experimental results. Without taking the approximations mentioned above, the pump-probe delay as a function of position is given by:

$$\tau(x) = \tau_0 + \frac{l(x)}{c} = \tau_0 + \frac{\sqrt{x^2 + z_0^2}}{c} \tag{S23}$$

where τ_0 is a constant shared by all photons that hit different areas on the sample, which will be set to be at the maximum changing rate of index, $\frac{dn}{dt}$. The small angle approximation is not taken either in the simulation. **Figure S6c** shows diagram of rays at different radius position of x that are focused on a spot at 147 mm away from the sample, which indicates that the ENZ film can work as an ultrafast lens with small spherical aberration when the pump beam is perfectly divergent, and the beam spot is not too large (no larger than hundreds of micrometers) to meet the paraxial approximation.

S5.2. Experimental verification of ultrafast lensing effect

The ultrafast lensing effect with the spatiotemporal gradient of index mentioned in S5.1. is verified with experiments by measuring the beam divergent angle change after interacting with the ITO film. Limited by the nature of the beam, there is a tradeoff between making the beam waist smaller and having a longer focal depth. As the size of our ITO film sample is small ($200\mu\mathrm{m} \times 200\mu\mathrm{m}$), it's challenging to focus the probe beam within the sample area and keep it well-collimated. We chose to focus the probe beam $5\mathrm{mm}$ upstream to the sample and make it slightly divergent on and after transmitting through the ITO film (**Figure S6a**). As a reference, if a lens with the focal length of $147\mathrm{mm}$ as simulated in S5.1. is located on the position of the ITO film, the beam spot size will be reduced by 6% in the far field (**Figure S6b**).

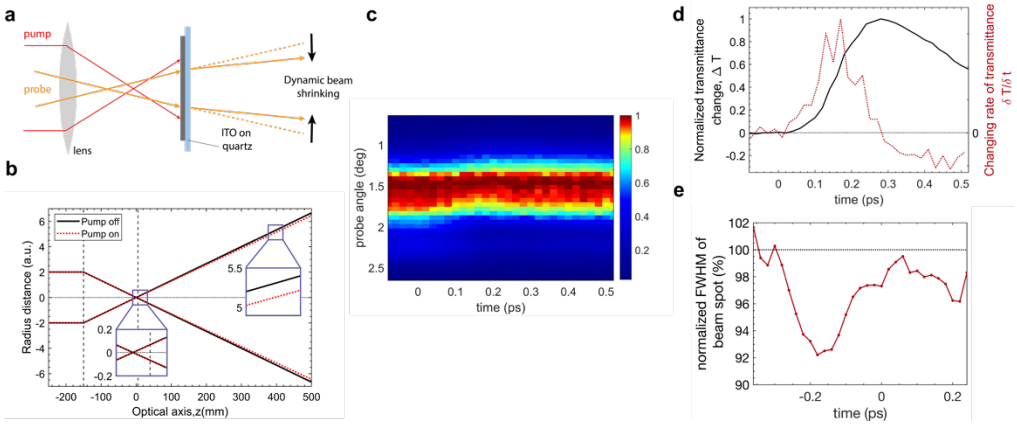

Figure S6 a Diagram of pump and probe beam: The pump beam is focused 3mm upstream of the sample, with a common lens (f=150mm), to be divergent on the ITO film. The probe beam is focused 6mm upstream to the sample, with a smaller beam spot on the ITO film. The spatiotemporal gradient at the rising edge of the dynamic index change is expected to work as a positive lens to make the probe beam less divergent. b Ray diagram, with a lens (f=89mm, as simulated from the spatiotemporal index gradient generated beam steering) on the position of the sample. c Normalized intensity distribution along the angular direction, as a function of pump-probe delay. The intensity of probe beam is measured by scanning a photodiode along the angular axis. d The transmissivity change (ΔT), changing rate of transmissivity ($\delta T/\delta t$) and e The beam spot size (full width at 60% of maximum) of probe beam spot as a function of pump-probe delay, which indicates that beam shrinking is maximized at the pump-probe delay with maximum changing rate of index.

A photodiode Is used to scan along the angular direction of probe beam, at 432 mm away from the ITO film, to collect the angular distribution of the transmitted probe beam (**Figure S6c**), from which the results of the time-dependent beam spot size and its transmissivity are extracted (**Figure S6d,e**). The changing rate of transmissivity (**Figure S6d, red**) qualitatively indicates the changing rate of refractive index, $\delta n/\delta t$. It is observed that the maximized beam spot size change happens when $\delta n/\delta t$ is maximized. The 5.9% beam shrinking indicates an ultrafast lens with a focal length of 101 mm, which matches the focal length simulated from ultrafast beam steering in magnitude. The value of the focus effect can be overestimated (focal length to be underestimated) because of the inhomogeneous pump intensity, which is higher in the center of the pump beam spot for a Gaussian-like beam. It induces a larger transmissivity increase in the center part of the probe beam, which makes the angular distribution of the probe beam smaller and looks less divergent, contributing to a smaller focal length.

Supplementary references:

1. Alam, M. Z., De Leon, I. & Boyd, R. W. Large optical nonlinearity of indium tin oxide in its epsilon-near-zero region. Science (80-.). 352, 795–797 (2016).
2. Shaltout, A. M., Shalaev, V. M. & Brongersma, M. L. Spatiotemporal light control with active metasurfaces. Science (80-.). 364, (2019).
3. Jarrahi, M., Fabian, R., Pease, W., Miller, D. A. B. & Lee, T. H. High-speed optical beam-steering based on phase-arrayed waveguides. J. Vac. Sci. Technol. B Microelectron. Nanom. Struct. 26, 2124–2126 (2008).
4. Guo, X., Ding, Y., Duan, Y. & Ni, X. Nonreciprocal metasurface with space–time phase modulation. Light Sci. Appl. 8, (2019).
5. Shaltout, A., Kildishev, A. & Shalaev, V. Time-varying metasurfaces and Lorentz non-reciprocity. Opt. Mater. Express 5, 2459 (2015).
6. Larouche, S., Tsai, Y. J., Tyler, T., Jokerst, N. M. & Smith, D. R. Infrared metamaterial phase holograms. Nat. Mater. 11, 450–454 (2012).

7. Shaltout, A. M. et al. Doppler-shift emulation using highly time-refracting TCO layer. 2016 Conf. Lasers Electro-Optics, CLEO 2016 6–7 (2016).
8. Reshef, O., De Leon, I., Alam, M. Z. & Boyd, R. W. Nonlinear optical effects in epsilon-near-zero media. Nat. Rev. Mater. 4, 535–551 (2019).